



HAL
open science

MARSIS surface reflectivity of the south residual cap of Mars

Jeremie Mouginot, W. Kofman, A. Safaeinili, C. Grima, A. Null Herique, J.J. Plaut

► **To cite this version:**

Jeremie Mouginot, W. Kofman, A. Safaeinili, C. Grima, A. Null Herique, et al.. MARSIS surface reflectivity of the south residual cap of Mars. *Icarus*, 2009, 201 (2), pp.454. 10.1016/j.icarus.2009.01.009 . hal-00533497

HAL Id: hal-00533497

<https://hal.science/hal-00533497>

Submitted on 7 Nov 2010

HAL is a multi-disciplinary open access archive for the deposit and dissemination of scientific research documents, whether they are published or not. The documents may come from teaching and research institutions in France or abroad, or from public or private research centers.

L'archive ouverte pluridisciplinaire **HAL**, est destinée au dépôt et à la diffusion de documents scientifiques de niveau recherche, publiés ou non, émanant des établissements d'enseignement et de recherche français ou étrangers, des laboratoires publics ou privés.

Accepted Manuscript

MARSIS surface reflectivity of the south residual cap of Mars

Jeremie Mouginot, W. Kofman, A. Safaeinili, C. Grima, A. Herique,
J.J. Plaut

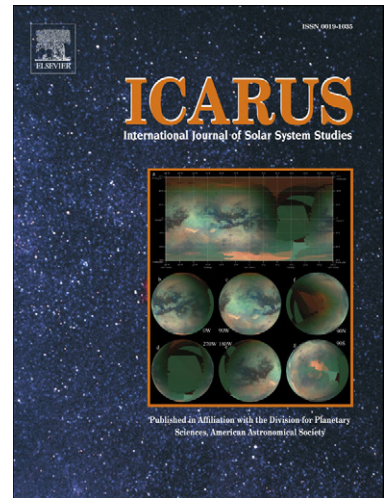
PII: S0019-1035(09)00031-1
DOI: [10.1016/j.icarus.2009.01.009](https://doi.org/10.1016/j.icarus.2009.01.009)
Reference: YICAR 8891

To appear in: *Icarus*

Received date: 1 July 2008
Revised date: 16 October 2008
Accepted date: 9 January 2009

Please cite this article as: J. Mouginot, W. Kofman, A. Safaeinili, C. Grima, A. Herique, J.J. Plaut, MARSIS surface reflectivity of the south residual cap of Mars, *Icarus* (2009), doi: 10.1016/j.icarus.2009.01.009

This is a PDF file of an unedited manuscript that has been accepted for publication. As a service to our customers we are providing this early version of the manuscript. The manuscript will undergo copyediting, typesetting, and review of the resulting proof before it is published in its final form. Please note that during the production process errors may be discovered which could affect the content, and all legal disclaimers that apply to the journal pertain.



1 **MARSIS surface reflectivity of the south residual cap**
2 **of Mars**

3 Mougnot J.¹, (jeremie.mougnot@obs.ujf-grenoble.fr)

4 Kofman W.¹, (wlodek.kofman@obs.ujf-grenoble.fr)

5 Safaeinili A.², (ali.safaeinili@jpl.nasa.gov)

6 Grima C.¹, (cyril.grima@obs.ujf-grenoble.fr)

7 Herique A.¹, (alain.herique@obs.ujf-grenoble.fr)

8 Plaut J. J.² (plaut@jpl.nasa.gov)

9

10

11 ¹Laboratoire de Planétologie de Grenoble, CNRS/UJF 38041 Grenoble Cedex, France

12 ²Jet Propulsion Laboratory, California Institute of Technology, Pasadena, CA 91109.

13

14

15

16

17

18

19

20 **Manuscript** : 13 pages

21 **Figures** : 5 pages

22 **Tables** : 1 page

23

24 **Proposed running head:**

25 MARSIS surface reflectivity of the South Residual Cap.

26

27 **The name and address to which editorial correspondence and proofs should be**

28 **directed:**

29 Jeremie MOUGINOT

30 122 rue de la piscine

31 38000 Grenoble

32 FRANCE

33 Jeremie.mouginot@obs.ujf-grenoble.fr

34

ACCEPTED MANUSCRIPT

35 **(Abstract)**

36 The south residual cap of Mars is commonly described as a thin and bright layer of
37 CO₂-ice. The Mars Advanced Radar for Subsurface and Ionospheric Sounding
38 (MARSIS) is a low-frequency radar on board Mars Express operating at the
39 wavelength between 55 and 230 m in vacuum. The reflection of the radar wave on a
40 stratified medium like the residual cap can generate interferences, causing weaker
41 surface reflections compared to reflections from a pure water ice surface.

42 In order to understand this anomalous low reflectivity, we propose a stratified
43 medium model, which allows us to estimate both the thickness and the dielectric
44 constant of the optically thin slab. First, we consider the residual cap as single unit
45 and show that the decrease in the reflected echo strength is well explained by a mean
46 thickness of 11 m and a mean dielectric constant of 2.2. This value of dielectric
47 constant is close to the experimental value 2.12 for pure CO₂-ice. Second, we study
48 the spatial variability of the radar surface reflectivity. We observe that the reflectivity
49 is not homogeneous over the residual cap. This heterogeneity can be modeled either
50 by variable thickness or variable dielectric constant. The surface reflectivity shows
51 that two different units comprise the residual cap, one central unit with high
52 reflectivity and surrounding, less reflective units.

53 **KEYWORD: RADAR OBSERVATIONS, MARS, POLAR CAPS, ICES**

54

55 **1. Introduction**

56

57 **1.1. South residual cap**

58

59 The south polar plateau of Mars is partially covered by a perennial thin layer of
60 carbon dioxide (CO₂) ice, which is easily visible from Earth and spacecraft due to its
61 high albedo compared to the surrounding regions. Astronomers have observed this
62 layer over a century [Flammarion 1892], but the composition (CO₂-ice) was
63 determined using Viking orbiter thermal data [Kieffer, 1979; Paige *et al.* 1990]. It has
64 been shown that this CO₂ layer directly lies above water ice (H₂O-ice), which
65 comprises the major part of the plateau [Plaut *et al.* 2007] in the form of South Polar
66 Layered Deposits (SPLD).

67 Thermal data from Thermal Emission Imaging System (THEMIS) revealed the
68 presence of small exposures of H₂O-ice adjacent to the CO₂-ice, based on temperature
69 signatures [Titus *et al.* 2003]. The Observatoire pour la Minéralogie, l'Eau, les
70 Glaces, et l'Activité (OMEGA) observed spectral signatures of both CO₂-ice and trace
71 amounts of H₂O-ice within the residual ice cap [Bibring *et al.* 2004, Douté *et al.*
72 2007]. OMEGA also confirmed the identification of H₂O-ice-rich surfaces near the
73 CO₂-ice cap

74 The perennial CO₂ deposit consists of numerous layers. Using Mars Global Surveyor
75 Mars Orbiter Camera (MOC) images, Thomas *et al.* [2005] showed that the south
76 residual cap consists of two distinct layered units, which were deposited at different

77 times, separated by a period of degradation. The older unit, about 10 m thick, has
78 layers approximately 2 m thick. The younger unit has variable numbers of layers,
79 each about 1 m thick.

80 An estimate of the quantity of CO₂ in the slab, which can be compared to the total
81 CO₂ content of the atmosphere, was made by Byrne and Ingersoll [2003]. They
82 showed that a CO₂ residual ice cap with 10 m thickness, an area of 87,000 km², and a
83 density of 1.6 g.cm⁻³, constitutes only about 5% of the average atmospheric mass.

84

85

86 **1.2. Surface Reflectivity measured by MARSIS**

87

88 MARSIS is a decameter-wave sounding radar, which can penetrate kilometers below
89 the icy surface. It has provided important results on the Martian subsurface [Picardi *et al.*
90 *et al.* 2005; Plaut *et al.* 2007; Watters *et al.* 2007] and ionosphere [Gurnett *et al.* 2005 ;
91 Duru *et al.* 2006; Safaeinili *et al.* 2007; Espley *et al.* 2007]. The radar uses four
92 frequency bands, which are centered at 1.8, 3, 4 and 5 MHz (166, 100, 75, and 60 m
93 wavelength). Each band has a width of 1 MHz.

94 The data have been corrected for the distortion (phase shift) [Safaeinili *et al.* 2003;
95 Mougnot *et al.* 2008a] and absorption [Mougnot *et al.* 2008b] due to the ionosphere.

96 The radar frequency is close to the plasma frequency (up to 4 MHz) of the ionosphere
97 [Nagy *et al.* 2004; Gurnett *et al.* 2005] and as a result the signal is broadened
98 significantly in addition to being delayed. This broadening of the pulses can cause
99 smearing of the resulting radargram. Correction for ionospheric effects is performed

100 to re-sharpen the pulses and compensate for the absorption effects as described in
101 Mougnot *et al.* [2008a].

102

103 We quantify the echo returned by the surface from MARSIS radargrams by localizing
104 the position in the radargram corresponding to the surface echo and measuring the
105 amplitude. The position corresponds to the surface elevation given by Mars Orbiter
106 Laser Altimeter (MOLA).

107 This surface echo amplitude (i.e., surface reflectivity) allows us to build reflectivity
108 maps in each MARSIS frequency band (map at 4 MHz in Fig. 1a; maps at other
109 frequencies show the same type of features). The map resolution is 14.7 km per pixel
110 (about the MARSIS footprint width). For bands centered at 3, 4 and 5 MHz, we used
111 305, 464 and 539 orbits, respectively, to construct reflectivity maps. For crossing
112 tracks, we average the data from multiple measurements from MARSIS is a nadir-
113 looking radar and the Mars Express polar orbit does not allow us to sound the surface
114 poleward of about 87°N and 87°S ; this lack of data results in a gap centered at the
115 pole.

116 To first order, the reflectivity is inversely correlated with the surface roughness,
117 because the power reflected by a surface at nadir decreases with its roughness. Thus
118 the topographic variations at lateral scales comparable to and/or larger than the
119 MARSIS wavelength are affecting the signal. This is normal behavior due to the loss
120 of coherency of the radar signal.

121 A simulator of returned radar echoes from Mars was developed by Nouvel et al.
122 [2004]. This computationally efficient radar signal simulation is based on the use of
123 the Facet Method as surface modeling scheme. The slope and the large-scale
124 roughness effects are simulated using MOLA topography to predict the surface echo
125 amplitude in each point [Nouvel et al. 2004]. In this simulation, the reflectivity

126 variability is only due to surface slopes, with an assumption of a single fixed surface
127 dielectric constant. It allows distinguishing dielectric and topographic effects.

128 For each MARSIS radargram, we generate the corresponding radar simulation and
129 extract the surface amplitude from simulated radargrams to obtain a simulated
130 reflectivity map (Fig. 1b). We use identical procedures to generate both the simulated
131 map and the data map (Fig. 1a).

132 With such a simulated map, we can correct for any reflectivity variations that are due
133 to topographic effects. Indeed, the reflection coefficient (backscattering coefficient) R
134 can be written as the product of a dielectric constant function and a roughness
135 function [Ulaby et al. 1986], which is independent of the dielectric constant. By
136 normalizing the reflectivity map by the simulated one, we obtain a map proportional
137 to the dielectric constant (Fig. 1c). This normalization consists of the difference of the
138 power logarithms between data and simulated map. This normalized map reveals
139 variations of surface reflectivity across our area of interest. Indeed, one can see that
140 the region of the residual cap has very low reflectivity values (black box in Fig. 1c)
141 compared to the other parts of the SPLD.

142

143 **2. Wave propagation in a stratified medium**

144 We built a first order model to describe reflectivity in the south residual cap. This
145 model allows us to compute the radar wave propagation in a stratified medium and
146 then obtain a corresponding reflectivity.

147 Previous work indicates that the south residual cap consists of a thin perennial slab of
148 CO₂-ice overlapping H₂O-ice. So we model the south residual cap reflectivity using
149 three layers: the atmosphere, the CO₂-ice and the H₂O-ice (Fig. 2).

150 In a two-layer medium with refractive indices n_i and n_j , the reflection coefficient for
 151 normal incidence is given by the equation:

$$152 \quad r_{ij} = \frac{n_j - n_i}{n_j + n_i} \quad (1)$$

153 In a stratified medium (i.e., with three layers in our case), the reflection coefficient
 154 equation may be conveniently expressed in terms of the corresponding coefficients r_{12}
 155 and r_{23} associated with the reflection coefficients at the first and the second interface,
 156 respectively [Born and Wolf 1959]:

$$157 \quad r = \frac{r_{12} + r_{23}e^{2i\beta}}{1 + r_{12}r_{23}e^{2i\beta}} \quad (2)$$

158 where $\beta = \frac{2\pi}{\lambda}n_2h$, h is the thickness of the intermediate layer and λ is the
 159 wavelength of the incident wave. r_{12} , r_{23} may be obtained by substituting equation 1
 160 with the corresponding subscripts. This notation implies that n_1 , n_2 and n_3 are
 161 respectively, the refractive index for the upper (atmosphere), intermediate (CO₂ slab)
 162 and lower (H₂O-ice) layers (see Fig. 2). This model does not include any losses in the
 163 media, which, we believe, is a good approximation because for CO₂- and H₂O-ice
 164 losses are known to be weak. In addition polar MARSIS measurements typically
 165 show low losses [Plaut *et al.*, 2007]. The refractive index n_i corresponds to the square
 166 root of the real part of dielectric constant: $n_i = \sqrt{\epsilon_i}$.

167

168 As the MARSIS radar signal has a bandwidth of 1 MHz and therefore is not
 169 monochromatic, we cannot limit ourselves to equation 2 to obtain the reflectivity.
 170 Instead, we have to calculate the reflectivity as:

$$171 \quad R = \max \left(\left\| \text{IFFT}(S(f)r(f)S^*(f)) \right\|^2 \right) \quad (3)$$

172 where f is the frequency, r is the reflection coefficient defined in equation 2 and S is
173 the linearly modulated chirp signal of MARSIS. Equation 3 describes our method to
174 model the amplitude of the surface echo: we apply to an ideal transmitted signal
175 (chirp) the reflection coefficient $r(f)$. The Inverse Fast Fourier Transform (IFFT) gives
176 a time dependent signal that corresponds to the output of the matched filter of the
177 receiver.

178 In our model, we describe the H₂O-ice as compact pure water ice, which corresponds
179 to a dielectric constant ϵ_3 equal to 3.15. This value of pure water ice for the dielectric
180 constant is probably a good assumption, as previous workers have shown that the
181 deposits of the south polar-layered deposits are composed of relatively clean water ice
182 [Plaut *et al.* 2007; Zuber *et al.* 2007]. Moreover laboratory experiments have shown
183 that the real component varies between 3.14 and 3.19 [Ulaby *et al.* 1986] for various
184 types of “dirty ices”. In case of porous ice, the dielectric constant decreases. For
185 example, if the porosity of ice were equal to 10%, then, using Maxwell Garnett
186 mixing formulas [Sihvola, 1999], the dielectric constant would be 2.87. The dielectric
187 constant of the atmosphere is set to 1.

188 Fig. 3 presents the model of reflectivity R as function of the CO₂ thickness, h , for
189 different values of CO₂ dielectric constant. The two free parameters in our model are
190 h and the dielectric constant of the central layer ϵ_2 (the CO₂-ice). Both have an
191 impact on the inferred reflectivity. The CO₂ thickness in the plot is limited to the 0-20
192 m range because previous studies have shown that the global thickness is around 10
193 m.

194 First, we see on Fig. 3 that the reflectivity is minimal for a layer whose optical
195 thickness n_2h is close to $\lambda_0/4$ (λ_0 is the central wavelength) and the reflectivity is
196 maximal when optical thickness is close to $\lambda_0/2$ (Born and Wolf 1979).

197 Second, the reflectivity is minimum or strictly equal to zero when the dielectric
 198 constant of the intermediate layer is equal to $\sqrt{n_1 n_3}$. In our case, this corresponds with
 199 a dielectric constant of $\varepsilon_2 \cong 1.77$.

200 **3. Data Analysis**

201 **1.3. Comparison to H₂O-ice**

202 As the reflectivity measured by MARSIS is not absolutely calibrated, we have to
 203 compare the reflectivity in the south residual cap to a reference region of known
 204 composition.

205 We have chosen a reference region in the SPLD around the position 82°S and 150°W
 206 in a 2° by 2° box. It was chosen because of its flatness, so that we can expect that the
 207 only parameter that plays a role on the reflectivity is the dielectric constant. We know
 208 that the radar waves in the region are reflected by pure water ice, overlain by an
 209 optically thin soil layer [Plaut *et al.* 2007]. In this case, the reflection coefficient of
 210 the reference region is estimated as $r_{air/H_2O-ice} = 0.279$ with $\varepsilon_{H_2O-ice} = 3.15$ (see
 211 equation 1), which corresponds to a reflectivity $R = |r_{air/H_2O-ice}|^2 = 0.078$.

212 In our modeling effort, we consider the south residual cap according to the geological
 213 unit defined by Skinner *et al.* [2006] in the Mars geologic maps. MARSIS
 214 measurements cover about 60% of the 87,000 km² the south residual cap (to 87°S).
 215 We select all MARSIS reflectivity measurements that are either within the south
 216 residual cap or in the reference region. We obtain a distribution (see Fig. 4) of the
 217 reflectivity for both regions and for each of the three MARSIS frequency bands. The
 218 band 1 centered at 1.8 MHz is not used because of the low amount of data.

219 In order to find the most probable reflectivity values that characterize each region, we
220 fit this distribution by a Gaussian function. Best-fit parameters are summarized in
221 Table 1. Results show that for all frequencies, the reflectivity is much lower in the
222 south residual cap than in the reference region.

223 In order to find the best values for model parameters (ε , thickness) that reproduce the
224 observations, we use the model described previously. We fix a range for these
225 parameters, which are from 0 to 20 m for the thickness and from 1.0 to 3.15 for the
226 dielectric constant. The limits for the dielectric constant are the dielectric constant of
227 the upper and lower media (i.e. respectively the atmosphere and the water ice). The
228 procedure consists of a minimization between the model of reflectivity in a stratified
229 medium and the MARSIS measurements for all frequency bands simultaneously.

230 Application of this procedure gives the best value in our model of a mean thickness of
231 11 m and a mean dielectric constant of 2.3. This CO₂ dielectric constant is close to the
232 value measured by Pettineli *et al.* [2003] of 2.12. It confirms that the thin bright slab
233 in the south residual cap is primarily CO₂-ice. The formal 1-sigma errors on each
234 parameter, computed from the covariance matrix in the minimization, are 1 m for the
235 thickness and 0.2 for the dielectric constant.

236

237 **1.4. Local Study**

238 In this section, we are not considering the south residual cap as a single unit, but we
239 try to evaluate, locally, (with a resolution of about 14.7 km) the properties of the CO₂
240 slab. One can see in Fig. 1c that there is a large variability of reflectivity in the
241 residual cap.

242 Within our model representation, these variations can be explained as a change in
243 thickness or change in the dielectric constant. In the previous section, we use all the
244 data in the residual cap and so the statistics are robust. This allows us to easily extract
245 the mean behavior. However, in the local study, the statistics for each bin are poor and
246 it is difficult to invert the two parameters at the same time because they play a similar
247 role in reducing the reflectivity of the surface. Alternatively, we can fix one parameter
248 and solve for the other one. Thus for each pixel, we try to describe the reflectivity
249 variation as a change in dielectric constant only, or as a change in CO₂-ice thickness
250 only.

251 **1.1.1. Spatial Variability of the dielectric constant?**

252 First, we fix the thickness at 10 meters and look at the changes in the dielectric
253 constant due to variation of the reflectivity. The resulting dielectric map is shown in
254 Fig. 5a. One can see that the low reflectivity regions (Fig. 1c) correspond to areas
255 where the dielectric constant is close to the value of pure CO₂-ice (2.12) [Pettineli *et*
256 *al.* 2003]. The central part of the residual cap corresponds to higher values of the
257 dielectric constant, between the CO₂-ice (2.12) and H₂O-ice (3.15) reflectivity values,
258 which means in this case a mixture between H₂O-ice and CO₂-ice. This mixture could
259 be intimate (at the grain size level) or, because MARSIS has a large footprint, CO₂
260 residual cap and water outcrop reflectivity can be mixed in the returned signal. Using
261 the Maxwell Garnett mixing formula [Sihvola, 1999] and supposing that the effective
262 dielectric constant is only due a mixing between H₂O- and CO₂-ice, we obtain the
263 percentage of CO₂-ice compared to H₂O-ice. Fig. 5a shows that the ice content in the
264 central part could be up to 50% of H₂O, whereas surrounding terrains would contain
265 less than 20%.

266 **1.1.2. Spatial Variability of the thickness?**

267 Next, we fix the CO₂ dielectric constant at 2.12 and estimate the thickness with our
268 model. This CO₂ dielectric constant is close to the previously found value and
269 corresponds to the value measured by Pettineli *et al.* 2003.

270 Fig. 5b shows the CO₂ thickness computed by our reflectivity model. In this
271 hypothesis, we observe on the Fig. 4b two types of terrains: terrains with relatively
272 low thickness in the central part (less than 6-7m thick) and higher thickness in the
273 surrounding terrains (about 12 m thick). As it is difficult to measure a 1 dB decrease,
274 thicknesses under 4 m cannot be extracted from our analysis.

275

276 **4. Discussion**

277 **1.5. Errors**

278 In this section, we discuss possible errors in our method.

279 In the first part of the analysis, where we study the general reflectivity of the residual
280 cap, we make an assumption of the constant dielectric of the reference region. For
281 example, if there is a porosity in the shallow subsurface of the ice sheet, the dielectric
282 constant of the reference would decrease and so the reflectivity. For 10% porosity,
283 ϵ_{H_2O-ice} would be 2.87 and the corresponding reflectivity would be $R = 0.066$. A

284 porosity of 10% in water ice would thus reduce the reflectivity less than 1 dB.

285 Our model assumes no porosity for water ice (i.e. $\epsilon_{H_2O-ice} = 3.15$) and we think that
286 the assumption does not have a significant effect on our results. Our model is not
287 particularly sensitive to this parameter. For the 10%-porosity case, the output values
288 of the model would be still 11 m for the thickness and 2.2 for the dielectric constant of

289 the CO₂. This change is inside the uncertainties given by the 1-sigma errors on each
290 parameter.

291 In the second part, where we study the spatial variability in the south residual cap, we
292 cannot exclude that the effect of roughness at about tens of meters scale could explain
293 the reflectivity variability. However we think that the geologic features in the residual
294 cap (depressions of few meters) are small compared to the MARSIS wavelength and
295 are not responsible for the decrease in reflectivity.

296

297

298 **1.6. Conclusions**

299

300 The multi-layered reflection model proposed in this paper allows us to estimate a CO₂
301 slab thickness for a portion of the south residual cap of Mars. The mean CO₂
302 thickness measured by MARSIS seems to be in agreement with the thickness
303 estimated by Thomas *et al.* 2005.

304 It is interesting to note that the reflectivity detected by MARSIS is not homogenous
305 across the residual cap. Indeed we observe that the central part of the residual cap has
306 higher reflectivity than surrounding areas.

307 We have proposed an interpretation of this heterogeneity in terms of dielectric
308 constant and thickness of the CO₂-ice slab.

309 Firstly, supposing that the thickness is constant across the residual cap and solving for
310 dielectric variations, we would conclude that the central part is a mixture of CO₂ and
311 H₂O ices, and the surrounding terrains are mainly pure CO₂-ice.

312

313 Alternatively, supposing that the residual cap composition is homogeneously pure

314 CO₂-ice and solving for thickness variations, it appears that the central terrains are
315 thinner than the surrounding terrains. In this case, the volume of CO₂-ice contained in
316 the mapped part of the residual cap is about $4.1 \times 10^{11} \text{ m}^3$. As MARSIS measurements
317 cover 60% of the residual cap, we can estimate that the total volume $6.85 \times 10^{11} \text{ m}^3$,
318 which corresponds to about 5% (0.27 mbar) of atmospheric surface pressure (5.6
319 mbar) if we assume that the CO₂-ice density is about 1.6 g.cm^3 . This estimation is
320 consistent with previous works that predict that the amount of CO₂ in the residual cap
321 is small compared to the mass of the atmosphere [Prettyman *et al.* 2004; Byrne and
322 Ingersoll, 2003].

323 In both cases, our model shows that the central part of the mapped portion of the
324 residual cap, which shows lower surface reflectivity, contains less CO₂-ice than the
325 surrounding parts of the residual cap.

326 A similar analysis could be conducted with the SHallow subsurface RADar
327 (SHARAD), which operates at 20 MHz (i.e., a wavelength of 15 m in vacuum). The
328 SHARAD horizontal resolution is 300 m, which would allow description of the
329 surface features at a better resolution. SHARAD may also be sensitive to the seasonal
330 CO₂ deposits when the thickness is 1-2 m as described by Nunes and Phillips 2006.,
331 although this study is probably more difficult because SHARAD is more sensitive to
332 meter-scale roughness.

333

334 **Acknowledgments**

335

336 The authors acknowledge the French space agency (CNES) for support of these
337 studies in Laboratoire de Planétologie de Grenoble. Operations of the Mars Express
338 spacecraft by the European Space Agency (ESA) are gratefully acknowledged. Lynn
339 Carter and an anonymous reviewer provided helpful suggestions for this paper.

340

ACCEPTED MANUSCRIPT

341 **References**

342

343 Bibring, J., and 13 colleagues, 2004. Perennial water ice identified in the south polar
344 cap of Mars , Nature 428, 627-630.

345

346 Born M. and Wolf E., 1979. Principles of Optics: Electromagnetic theory of
347 propagation, interference and diffraction of light, Cambridge Univ. Press, Cambridge,
348 UK.

349

350 Byrne, S. and Ingersoll, A. P., 2003. A Sublimation Model for Martian South Polar
351 Ice Features, Science 299, 1051-1053.

352

353 Douté, S. Schmitt, B., Langevin, Y., Bibring, J.-P., Altieri, F., Bellucci, G., Gondet,
354 B., Poulet, F. & the MEX OMEGA team, 2007. South Pole of Mars: Nature and
355 composition of the icy terrains from Mars Express OMEGA observations, Planetary
356 And Space Science 55, 113-133.

357

358 Duru, F.; Gurnett, D. A.; Averkamp, T. F.; Kirchner, D. L.; Huff, R. L.; Persoon, A.
359 M.; Plaut, J. J. & Picardi, G., 2006. Magnetically controlled structures in the
360 ionosphere of Mars, J. Geophys. Res. 111, A12204.

361

362 Espley, J. R., Farrell, W. M., Brain, D. A., Morgan, D. D., Cantor, B., Plaut, J. J.,
363 Acuña, M. H., Picardi, G., 2007. Absorption of MARSIS radar signals: Solar
364 energetic particles and the daytime ionosphere, Geoph. Res. Let. 34, 9101-+.

365

366

367 Flammarion, C., 1892. La planète mars et ses conditions d'habitabilité, v. 1.

368 Gauthier–Villars et Fils, Paris.

369

370 Gurnett, D.A. and 11 colleagues, 2005. Radar soundings of the ionosphere of Mars,

371 Science 310, 1929–1933.

372

373 Kieffer, H.H., 1979. Mars south polar spring and summer temperatures: a residual

374 CO₂ frost, J. Geophys. Res. 84, 8263–8288.

375

376 Mougnot, J.; Kofman, W.; Safaeinili, A.; Herique, 2008a. A Correction of the

377 ionospheric distortion on the MARSIS surface sounding echoes, Planetary and Space

378 Science 56, 917-926.

379

380 Mougnot, J.; Kofman, W.; Safaeinili, A.; Herique, A.; Plaut, J. J.; Picardi, G., 2008b.

381 Calibration of MARSIS Surface Echoes LPSC XXXIX, No. 1391, p. 1716

382

383 Nouvel, J. F.; Herique, A.; Kofman, W., Safaeinili, A., 2004. A. Radar signal

384 simulation: Surface modeling with the Facet Method, Radio Science 39, RS1013.

385

386 Nunes, D. C., Phillips, R. J., 2006. Radar Subsurface Mapping of the Polar Layered

387 Deposits on Mars J. Geophys. Res. 111, 6+-.

388

389 Paige, D., Herkenhoff, K., Murray, B., 1990. Mariner 9 observations of the south

390 polar cap of Mars: evidence for residual CO₂ frost. J. Geophys. Res. 95, 1319–1335.

391

392 Pettinelli, E.; Vannaroni, G.; Cereti, A.; Paolucci, F.; Della Monica, G.; Storini, M. &

393 Bella, F., 2003. Frequency and time domain permittivity measurements on solid CO₂394 and solid CO₂-soil mixtures as Martian soil simulants, *J. Geophys. Res.* 108, 10-+

395

396 Picardi, G. and 12 colleagues, 2004. Performance and surface scattering models for

397 the Mars Advanced Radar for Subsurface and Ionosphere Sounding (MARSIS)

398 *Planet. and Space Science* 52, 149-156.

399

400 Plaut, J. J. and 23 colleagues, 2007. Subsurface Radar Sounding of the South Polar

401 Layered Deposits of Mars, *Science* 316, 92-.

402

403 Prettyman, T. H. and 12 colleagues, 2004. Composition and structure of the Martian

404 surface at high southern latitudes from neutron spectroscopy, *J. Geophys. Res.* 109,

405 5001-+

406

407 Safaeinili, A.; Kofman, W.; Nouvel, J.; Herique, A., Jordan, R. L., 2003. Impact of

408 Mars ionosphere on orbital radar sounder operation and data processing, *Planetary*409 *and Space Science* 51, 505-515.

410

411 Safaeinili, A.; Kofman, W.; Mouginot, J.; Gim, Y.; Herique, A.; Ivanov, A. B.; Plaut,

412 J. J., Picardi, G., 2007. Estimation of the total electron content of the Martian

413 ionosphere using radar sounder surface echoes, *Geophysical Research Letters* 34,

414 23204-+.

415

- 416 Skinner, J.A., Jr., Hare, T.M., Tanaka, K.L., 2006, Digital Renovation of the Atlas of
417 Mars 1:15,000,000-Scale Global Geologic Series Maps, LPSC XXXVII, abstract
418 #2331
419
- 420 Sihvola A. , 1999. Electromagnetic mixing formulas and applications, IEE
421 Electromagnetic waves series 47, The institution of Electrical Engineers.
422
- 423 Ulaby, F.T., Moore, R.K., Fung, A.K., 1986. Microwave Remote Sensing Active and
424 Passive, Artech House, Volume II.
425
- 426 Watters, T. R. and 12 colleagues, 2007. Radar Sounding of the Medusae Fossae
427 Formation Mars: Equatorial Ice or Dry, Low-Density Deposits?
428 Science, 318, 1025.
429
- 430 Zuber, M. T.; Phillips, R. J.; Andrews-Hanna, J. C.; Asmar, S. W.; Konopliv, A. S.;
431 Lemoine, F. G.; Plaut, J. J.; Smith, D. E. & Smrekar, S. E., 2007. Density of Mars
432 South Polar Layered Deposits, Science 317, 1718-.

433 **Tables**

434

| Center of the Gaussian | 3 MHz | 4 MHz | 5 MHz |
|---|--------------|--------------|--------------|
| South residual cap | -13.1 | -14.1 | -15.5 |
| Surface reference [H₂O-ice] | -7.5 | -8.5 | -8.3 |
| Reflectivity decrease | 5.6 | 5.5 | 7.2 |

435

436 **Table Captions**

437

438 Table 1: The table summarizes the result of the Gaussian fit made on the distribution
 439 presented in Fig. 4. The two first lines show the reflectivity (in dB) of the central
 440 position of the Gaussian (for the residual cap and for the reference region,
 441 respectively). The last line corresponds to the difference (in dB) between reference
 442 and residual cap.

443

444 **Figure Captions**

445

446 Fig. 1: (a) Surface reflectivity map from MARSIS using the radar frequency centered
447 at 4 MHz. The projection is polar stereographic. The reflectivity is represented in
448 decibel scale. (b) Simulated reflectivity map using MOLA topography. The
449 simulation is performed with a constant $\epsilon_{surface}$. (c) Surface reflectivity map at 4 MHz
450 normalized by the simulated reflectivity map. (d) Mars Orbiter Camera (MOC) wide-
451 angle mosaic map of the south polar region of Mars. The map resolution is about 14.7
452 km per pixel.

453

454 Fig. 2: Schematic view of a vertical ground section of the south residual cap, as
455 described in our model.

456

457 Fig. 3: Reflectivity R of the layered surface (see Fig. 2) as a function of the thickness
458 h for different values of the dielectric constant ϵ_{CO_2} . The dielectric constants of the
459 upper and lower medium are 1 and 3.15, respectively.

460

461 Fig. 4: The distribution of surface reflectivity in the reference region (dark grey) and
462 the south residual cap (light grey). The black dashed lines are the Gaussian fit made
463 on the distribution. The results of the fit are summarized in Table 1.

464

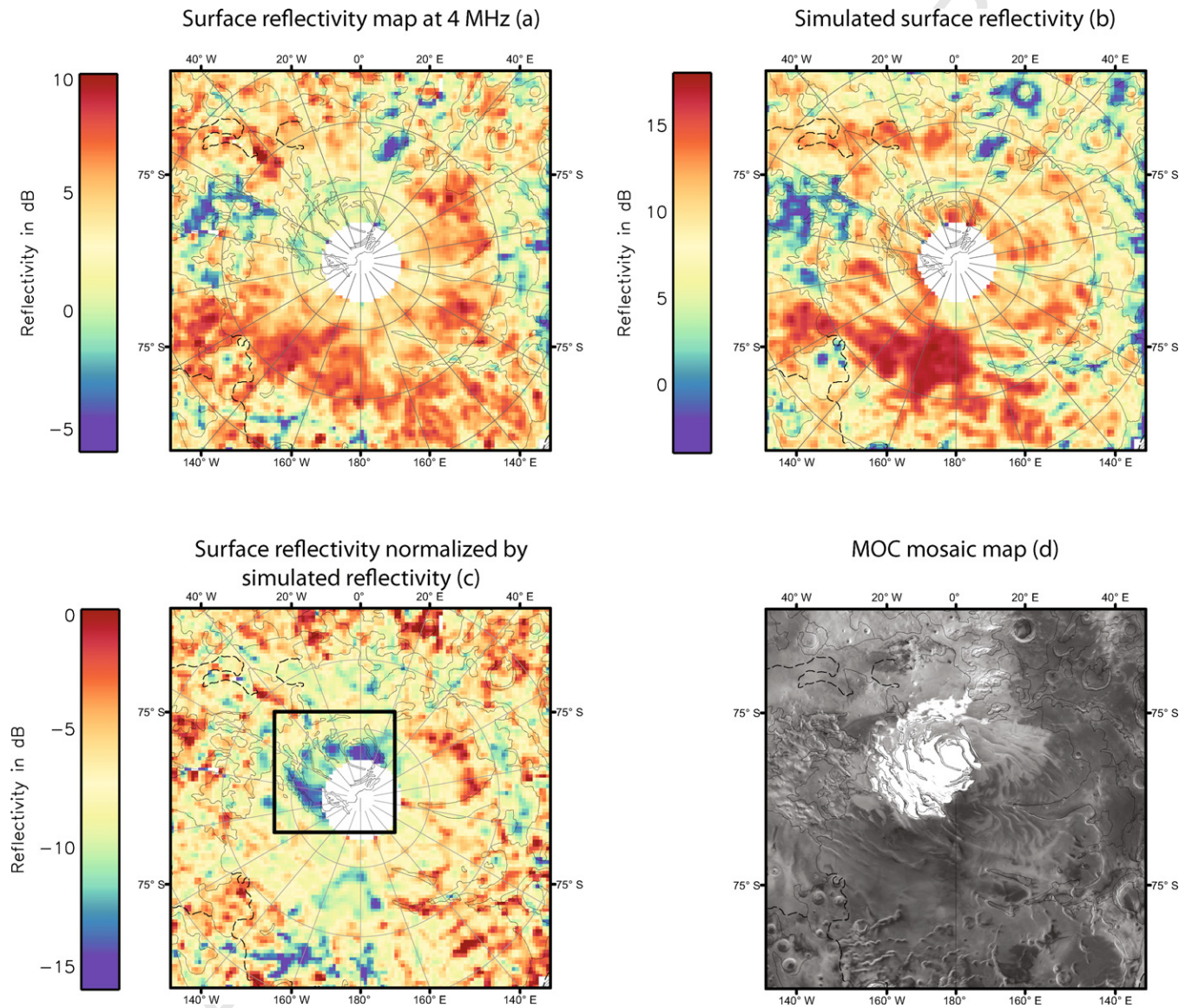
465 Fig. 5: Maps of the south residual cap region. (a) Map of the dielectric constant found
466 by our reflectivity model with the thickness fixed at 10 meters. Using the Maxwell
467 Garnett mixing formula [Sihvola, 1999] and assuming that the effective dielectric

468 constant is only due to mixing between H₂O- and CO₂-ice, we give the percentage of
469 CO₂-ice and H₂O-ice. (b) Map of the CO₂ thickness found by our model with
470 dielectric constant fixed at 2.12.

471

472

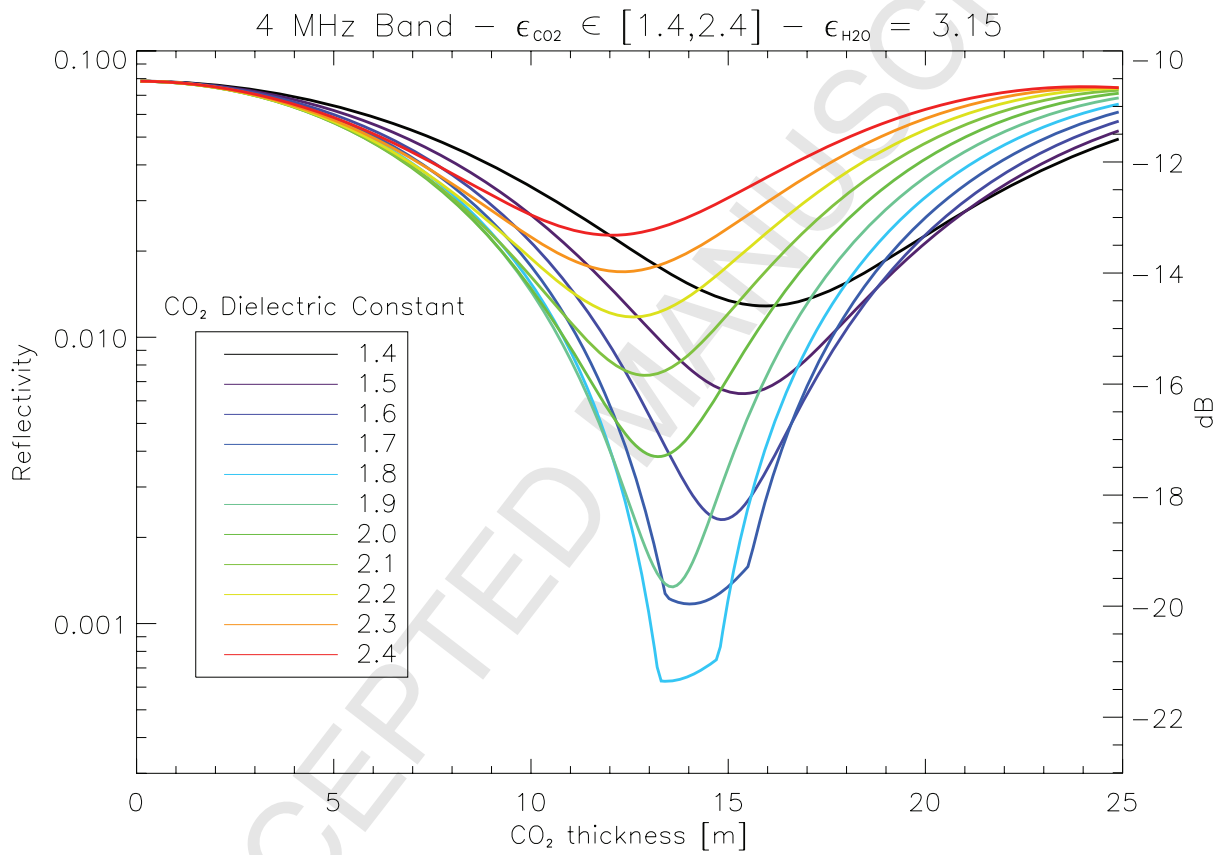
ACCEPTED MANUSCRIPT

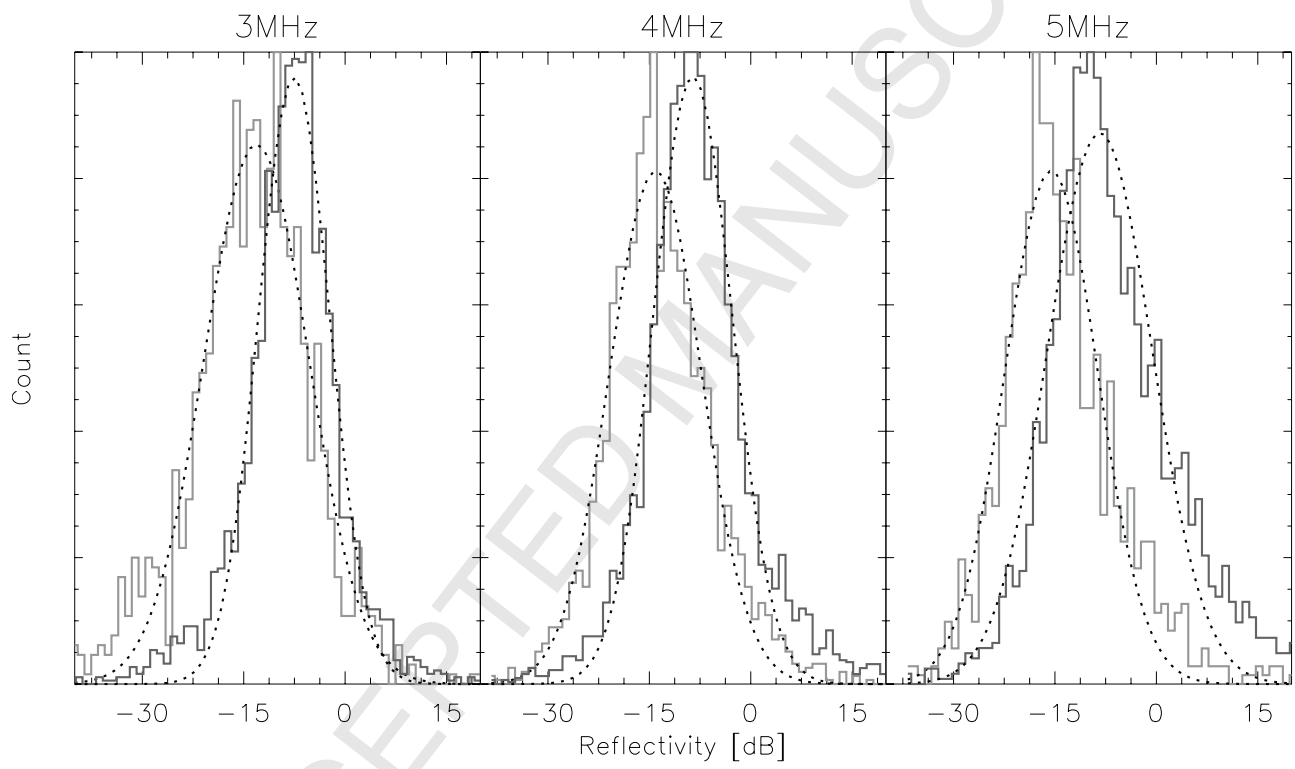


$\epsilon_{1r}=1$ Atmosphere

ϵ_{2r} Bulk CO₂ ice h

$\epsilon_{3r}=3.15$ Water ice





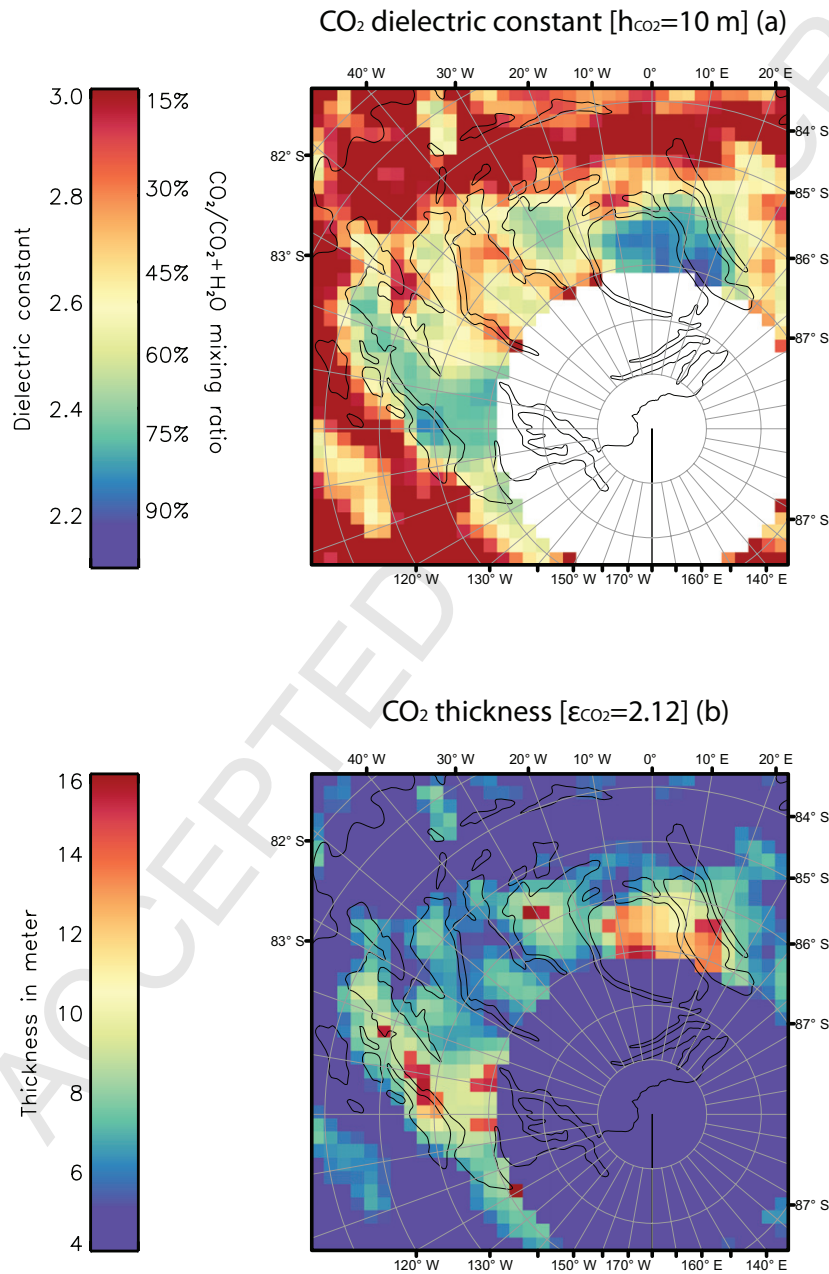


Figure 5 - Mougnot (2008)